Received: 6 March 2024 | Revised: 1 July 2024 | Accepted: 20 August 2024

DOI: 10.1002/hbm.70015

RESEARCH ARTICLE

WILEY

Body mass index associated with respiration predicts motion in resting-state functional magnetic resonance imaging scans

Shishi Huang[1] | Andrew D. Vigotsky[2,3] | Apkar Vania Apkarian[4,5] | Lejian Huang[4,5]

[1]Department of Neurology, The Second Affiliated Hospital and Yuying Children's Hospital of Wenzhou Medical University, Wenzhou, China

[2]Department of Biomedical Engineering, Northwestern University, Evanston, Illinois, USA

[3]Department of Statistics, Northwestern University, Evanston, Illinois, USA

[4]Department of Neuroscience, Feinberg School of Medicine, Northwestern University, Chicago, Illinois, USA

[5]Center for Translational Pain Research, Feinberg School of Medicine, Northwestern University, Chicago, Illinois, USA

Correspondence
Lejian Huang and Apkar Vania Apkarian, Department of Neuroscience, Northwestern University, Chicago, IL 60611, USA.
Email: lejian-huang@northwestern.edu and a-apkarian@northwestern.edu

Funding information
National Institutes of Health, Grant/Award Number: 1P50DA044121-01A1; National Science Foundation, Grant/Award Number: DGE-1324585

Abstract

Decreasing body mass index (BMI) reduces head motion in resting-state fMRI (rs-fMRI) data. Yet, the mechanism by which BMI affects head motion remains poorly understood. Understanding how BMI interacts with respiration to affect head motion can improve head motion reduction strategies. A total of 254 patients with back pain were included in this study, each of whom had two visits (interval time = 13.85 ± 7.81 weeks) during which two consecutive re-fMRI scans were obtained. We investigated the relationships between head motion and demographic and pain-related characteristics—head motion was reliable across scans and correlated with age, pain intensity, and BMI. Multiple linear regression models determined that BMI was the main determinant in predicting head motion. BMI was also associated with two features derived from respiration signal. Anterior–posterior and superior–inferior motion dominated both overall motion magnitude and the coupling between motion and respiration. BMI interacted with respiration to influence motion only in the *pitch* dimension. These findings indicate that BMI should be a critical parameter in both study designs and analyses of fMRI data.

KEYWORDS
back pain, BMI, fMRI, motion, respiration signal

1 | INTRODUCTION

Head motion always exists during functional MRI (fMRI) acquisitions and is considered one of the major confounding factors impairing the quality of fMRI data and consequently reducing analytical efficiency (Ciric et al., 2018). So far, the most popular strategy to attenuate the effects of motion-related artifacts has been post-acquisition, identifying motion volume(s) or motion component(s) based on given motion-related threshold(s) and censoring or regressing them out from acquired fMRI data (Power et al., 2014; Pruim et al., 2015; Salimi-Khorshidi et al., 2014). In addition, prospective motion correction has been suggested (Lee et al., 1996), which measures head motion during image acquisition and updates sequence parameters in real-time, and has gradually played a role to improve quality of data (Hoinkiss et al., 2019; Hucker et al., 2021; Igata et al., 2017; Todd et al., 2015). Recently, some researchers have made efforts to develop pre-acquisition strategies, including behavioral interventions—e.g., before scanning, educating subjects to remain still during acquisition—and/or physically restraining the head from moving with medical tape or customized head molds (Krause et al., 2019; Power et al., 2019).

The finding that patients with back pain have greater head motion than healthy controls (Huang et al., 2019; Yang et al., 2021) led us to

investigate how and to what extent demographic and pain-related characteristics of the patients correlate with head motion. By explicating these relationships, we hoped to develop an optimal combination of pre- and post-acquisition strategies to mitigate motion effects.

Head motion can be conceptualized as a neurobehavioral trait, which is correlated with numerous demographic phenotypes, including body mass index (BMI) (Couvy-Duchesne et al., 2014; Hodgson et al., 2017; Zeng et al., 2014). Ekhtiai et al. demonstrated that BMI explains an appreciable amount of motion variance during scanning, and Beyer et al. went a step further to reveal that decreasing BMI reduces head motion (Beyer et al., 2020; Ekhtiari et al., 2019). A causal link between BMI and motion combined with obesity's interference with respiratory function (Mafort et al., 2016) suggests motion, BMI, and respiration are closely intertwined. However, to the best of our knowledge, this relationship has not yet been investigated. To improve pre-acquisition head motion reduction strategies, we need to better understand how BMI and respiration interact to affect head motion.

In this paper, we start by investigating the relationships between motion and demographic and pain-related characteristics. Next, we fit multiple linear regression models to evaluate predictors of head motion. In the end, after two parameters were derived from the respiration signal, the relationship between motion, BMI, and respiration was further elucidated.

2 | METHODS

2.1 | Participants

A total of 254 patients with back pain were included in this project (133 males, 121 females; age range and its (mean ± SD) were [21, 88] and (52.81 ± 14.05) years old, respectively). These patients were recruited across three randomized trials assessing the efficacy of chronic pain treatments (Pinto et al., 2023; Reckziegel et al., 2021; Tetreault et al., 2016). Participants were excluded if they (1) were less than 18 or greater than 85 years old; (2) reported a history of head injury and/or cerebral disease (e.g., stroke or encephalopathy); (3) had diabetes or a psychiatric disease; (4) reported a history of brain neurosurgical procedures and/or epilepsy; (5) were unable to cooperate (e.g., psychogenic or cognitively impaired); (6) reported pregnancy, drug dependence, or drug abuse; (7) were not suitable for MRI scan.

Participants visited the lab twice. At each visit, we obtained one structural and two consecutive rs-fMRI images. The range and mean ± SD of the time between the two visits were [5, 35] and 14 ± 8 weeks, respectively. During the first visit, participants completed a battery of self-report demographic and pain-related questionnaires, including age, gender, weight and height, pain intensity, and pain duration. BMI was calculated from weight and height and its mean ± SD was 29.28 ± 5.69. Pain intensity was rated by numerical rating scale (NRS) (Farrar et al., 2001) prior to scans, where 0 corresponds to no pain and 100 indicates worst possible pain, and its mean ± SD was 62.05 ± 19.43 at first visit and 47.52 ± 27.37 at second visit. The demographic and pain-related characteristics of the participants are summarized in Table 1. In this study, BMI was assumed to be constant between two visits. Herein, we abbreviate rs-fMRIs as V1R1 (visit 1, resting 1), V1R2 (visit 1, resting 2), V2R1 (visit 2, resting 1), and V2R2 (visit 2, resting 2). The number of participants included in data analyses at each stage was 254 (V1R1), 174 (V1R2), 183 (V2R1), and 114 (V2R2), respectively, among which 84 (V1R1), 71 (V1R2), 54 (V2R1), and 40 (V2R2) participants remained for respiration features being extracted.

TABLE 1 Demographic and pain-related characteristics of patients with back pain.

Patients with back pain ($N = 254$)		
Age (y/o), mean (SD)	52.81	(14.05)
Male, *N* (%)	133	(52.36)
BMI, mean (SD)	29.28	(5.69)
1st NRS, mean (SD)	62.05	(19.43)
2nd NRS, mean (SD)	47.52	(27.37)
Pain duration (weeks), median (min, max)	165	(1, 3147)
Interval time (weeks), mean (SD)	13.85	(7.81)

Abbreviations: BMI, body mass index; NRS, numerical rating scale; SD, standard deviation; y/o, years old.

The study was approved by the Institutional Review Board of Northwestern University, and all participants reviewed and signed a written informed consent.

2.2 | MRI scanning parameters

Participants were scanned on a clinical 3 Tesla Siemens Magnetom Prisma whole body scanner equipped with a 64 channel-head/neck coil. T1-anatomical brain images were acquired using integrated parallel imaging techniques (PAT; GRAPPA) with the following parameters: voxel size = 1 × 1 × 1 mm^3; TR/TE = 2.3 s/2.40 ms; flip angle = 9°; in-plane resolution = 256 × 256; slices per volume = 176; field of view = 256 mm. Rs-fMRI images were acquired with the following parameters: TR/TE = 555/22 ms; flip angle = 47°; voxel size = 2 × 2 × 2 mm^3; in-plane resolution = 96 × 104; number of volumes = 1110; multiband accelerator = 8; number of slices = 64 acquired with interleaved ordering, which covers the whole brain from the cerebellum to the vertex.

To minimize head motion, a head support system consisting of two foam pads positioned on either side of the head was used with earplugs for reducing scanner noise. Participants were instructed to keep their eyes open and to remain as still as possible during acquisition.

During rs-fMRI scanning, a respiratory belt and pulse oximeter were sampled at 400 Hz to measure respiration and heart rate, respectively.

2.3 | Measurement of head motion

All volumes of a rs-fMRI were realigned to the middle of the time series, resulting in three rotational (*pitch*: shaking your head "Yes,"

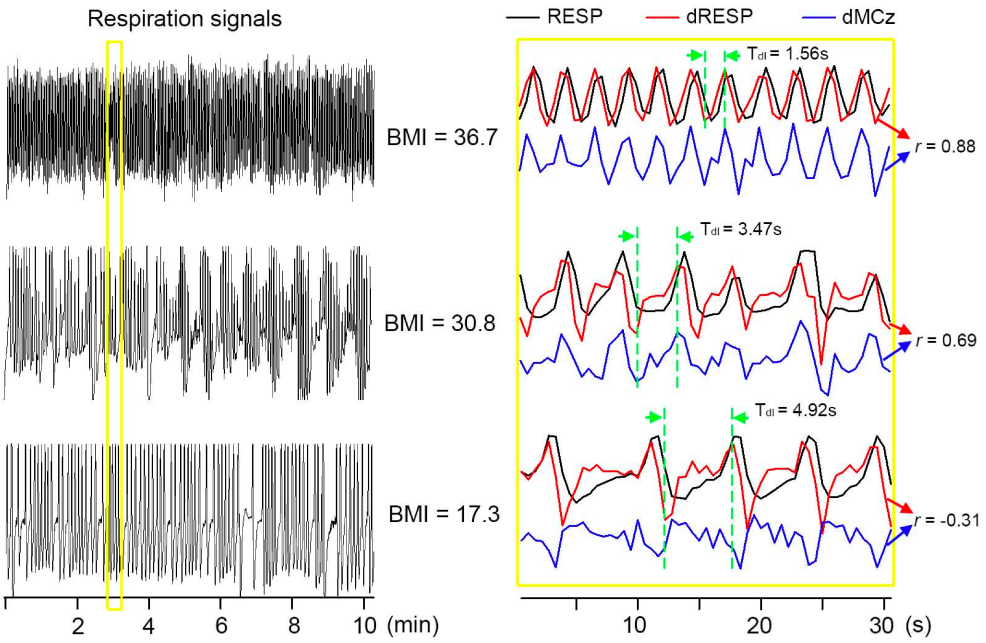

FIGURE 1 Illustration of two features derived from respiration signals in three subjects (BMI = 36.7, 30.8, and 17.3). The time between two dashed green lines is the time of differentiated inhalation (T_{dI}) in one respiration cycle. *r* is the Pearson correlation coefficient between dRESP and dMC in a given dimension (*pitch*, *roll*, *yaw*, *x*, *y*, *z*). RESP: respiration signals, black curves; dRESP: differentiated RESP, red curves; and dMC_z: motion in *z* dimension, blue curves. Note that the 30-s frame is a part of 11-min respiration signal.

sagittal; *yaw*: tilting to the left and right, frontal; and *roll*: shaking your head "No," transverse) and three translational (*x*: left–right, *y*: anterior–posterior, *z*: superior–inferior) motion correction (MC) parameters using MCFLIRT (Jenkinson et al., 2002). The differentiated six MC parameters—dMC_{dim}, $dim \in \Omega, \Omega = \{pitch, roll, yaw, x, y, z\}$—represent extent and direction of motion of one volume from one time point to the next (displacement) along each rotational or translational dimension. Framewise displacement (FD) of each dimension, FD_{dim}, was calculated as the absolute value of dMC_{dim}, respectively. These metrics capture the absolute displacement of each volume (except the first volume) along each dimension. To convert rotations of angular displacements to the units of translational displacements, the three rotational FDs were multiplied by 50 mm (Power et al., 2014). Mean framewise displacement (mFD) of each dimension—mFD_{dim}, was calculated as the average FD of each dimension across all time points except the first one, indicating the extent of head motion of each dimension over the duration of the scan. Total mean framewise displacement of each rs-fMRI data set, mFD_{total}, was calculated as the sum of above six mFDs, indicating the extent of head motion over the duration of the scan. This was repeated for all four scans. Since the distributions of framewise displacements were approximately lognormal, all values were log-transformed.

2.4 | Two features derived from respiration signal

During rs-fMRI scanning, imaging-synchronized respiration signals were collected using a respiration belt wrapped around the subject's chest through its transducer with a sampling rate of 400 Hz, amplitude of which was increased at the phase of inhalation and decreased at the phase of exhalation. The original signal, sampled at 50 Hz (divided by multiband accelerator, 8), was averaged over slices in each volume, resulting in a 1110-point smoothed respiration signal with a time resolution of 555 ms—the same as that of rs-fMRI scanning. The smoothed respiration signal of each subject was then *z*-scored. Subjects whose respiration signal was corrupted for at least half of the points were removed for further analysis.

For each subject, two features were derived from the *z*-scored respiration signal: mean time between differentiated inhalations (mT_{dI}) and maximum absolute values of Pearson's correlation coefficient between the differentiated respiration signal (dRESP) and dMC_{dim} across six motion dimensions ($|r|_{max}$). As shown in Figure 1, dRESP consisted of differences across inhalation signal and T_{dI} was defined as the time between the lowest and highest differentiated inhalation signal in a respiration cycle. After all peaks (lowest and highest time points) of the differentiated inhalation signal were identified by using a MATLAB function of *findpeaks*, mT_{dI} was calculated by averaging T_{dI}s over all cycles. $|r|_{max}$ was defined as follows:

$$|r|_{max} = \max_{dim \in \Omega} |correlation(dRESP, dMC_{dim})|,$$

where $\Omega = \{pitch, roll, yaw, x, y, z\}$, which represents the maximum coupling between the changes in MC and changes in the respiration signal. In this study, $|r|_{max}$ was Fisher *z*-transformed to stabilize its variance.

2.5 | Interaction between BMI and dRESP–dMC coupling and its effect on motion

The discovery that motion in the *y* and *z* dimensions dominated in both mFDs and the absolute value of Pearson's correlation between dRESP and dMC_{dim} ($|r_{dim}| = |correlation(dRESP, dMC_{dim})|$)

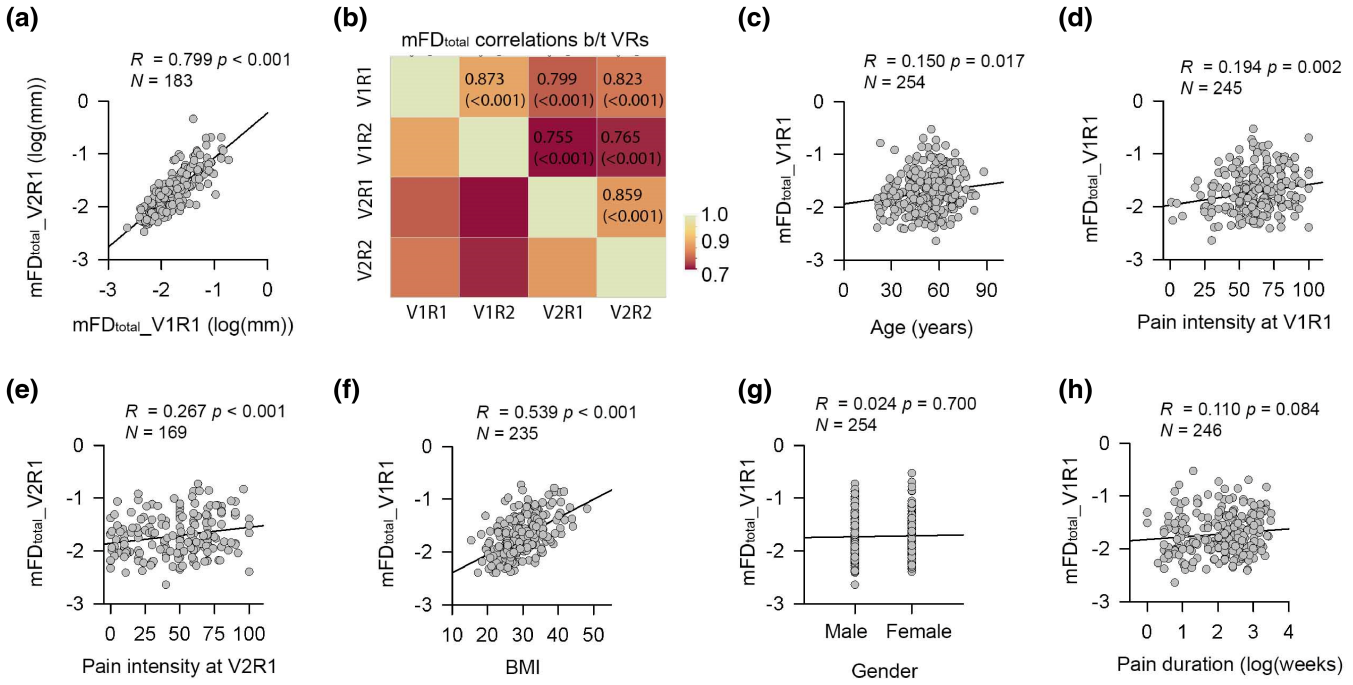

FIGURE 2 Motion was reliable across scans and significantly correlated with age, pain intensity, and BMI in patients with back pain. (a) Scatter plot of the correlation between log(mFD_{total}) from the first (V1R1) and second (V2R1) visits ($R = 0.799$, $p < 0.001$). (b) Heat map indicated the pair-wise correlation of mFD_{total} was consistent across scans (V1R1, V1R2, V2R1, and V2R2). (c) Scatter plot depicting the association between mFD_{total} of V1R1 and age ($R = 0.150$, $p = 0.017$). (d, e) Scatter plot of the relationships between mFD_{total} and pain intensity (NRS) at V1R1 ($R = 0.194$, $p = 0.002$) and V2R1 ($R = 0.267$, $p < 0.001$). (f) Scatter plot depicting the significant correlation between mFD_{total} of V1R1 and BMI ($R = 0.539$, $p < 0.001$). (g, h) No gender and pain duration effect on mFD_{total} of V1R1.

and the contour similarity of bar shape across dimensions between the motion and the $|r|_{max}$ inspired us to explore the relationship among motion represented by mFD_{dim}, BMI, and $|r_{dim}|$ (expounded in section 3.4). Since each participant had multiple data points (i.e., four scans), we had to account for this dependence in our model. Since we are interested in the so-called "population average" effect (i.e., across-rather than within-subjects), we opted to use a generalized estimating equation (GEE) to explore this relationship, which accounts for the covariance between data points (repeated scans). Here, we created a model to assess how BMI, $|r_{dim}|$, and their interaction affected mFD_{dim}, estimated using all four scans (V1R1, V1R2, V2R1, and V2R2) at once. The model was fit using a quasi-likelihood instead of maximum-likelihood estimation to estimate the parameters (Liang & Zeger, 1986) using *geepack* in R (Halekoh et al., 2006). GEEs exploit what is called a working correlation structure, which, in our case, adjusts the parameters' standard errors to account for dependence (repeated scans). Our GEE relied on the sandwich estimator to estimate the parameters' standard errors. The sandwich estimator relaxes some of the assumptions of standard linear regression by modeling residual dependence and heteroscedasticity. Importantly, our sample (and thus the number of clusters) was likely sufficiently large enough to overcome the sandwich estimator's small sample bias (Paik, 1988), which can inflate type I error rates and produce spurious findings with smaller sample sizes.

3 | RESULTS

3.1 | Relationships between motion and demographic variables

The extent of motion over the duration of the scan, represented by log(mFD_{total}), was reliable across all four scans (the range of correlation coefficient was between 0.755 and 0.859, all $p < 0.001$) (Figure 2a,b). The correlation between two consecutive rs-fMRIs (0.873 and 0.859) was greater than that between two visits (0.799 and 0.765). In addition, univariable GLM analysis revealed associations between motion and age ($R = 0.150$, $p = 0.017$; Figure 2c), pain intensity ($R = 0.194$, $p = 0.002$ at V1R1; Figure 2d and $R = 0.267$, $p < 0.001$ at V2R1; Figure 2e), and BMI ($R = 0.539$, $p < 0.001$; Figure 2f); however, neither gender ($R = 0.024$, $p = 0.700$; Figure 2g) nor log(pain duration) ($R = 0.110$, $p = 0.084$; Figure 2h) was statistically significantly associated with motion. Therefore, the extent of back pain patients' head motion resembled each other across scans and was significantly associated with age, pain intensity, and BMI.

3.2 | BMI as an independent predictor of motion

As shown in Table 2, a multiple regression analysis of motion with variables of BMI, age, pain intensity (NRS), log(pain

TABLE 2 Results of multiple regression analysis of mFD_{total} at V1R1.

Variables	β	SE	*t*-value	*p*-value	$-\log_{10}(p)$	Model fitting
BMI	0.032	0.004	8.67	**<0.001**	14.96	$F(5, 213) = 18.450$, $\mathbf{p < 0.001}$
Age	0.003	0.002	1.86	0.065	1.19	$R^2 = 0.303$, RMSE = 0.068 mm
Pain intensity	0.001	0.001	0.88	0.301	0.42	
Pain duration (log(weeks))	0.023	0.028	0.83	0.506	0.39	
Gender (male = 0, female = 1)	−0.002	0.042	−0.38	0.704	0.15	

Note: Bold *p*-value represents significant from the statistical analysis (*p*-value < 0.05).

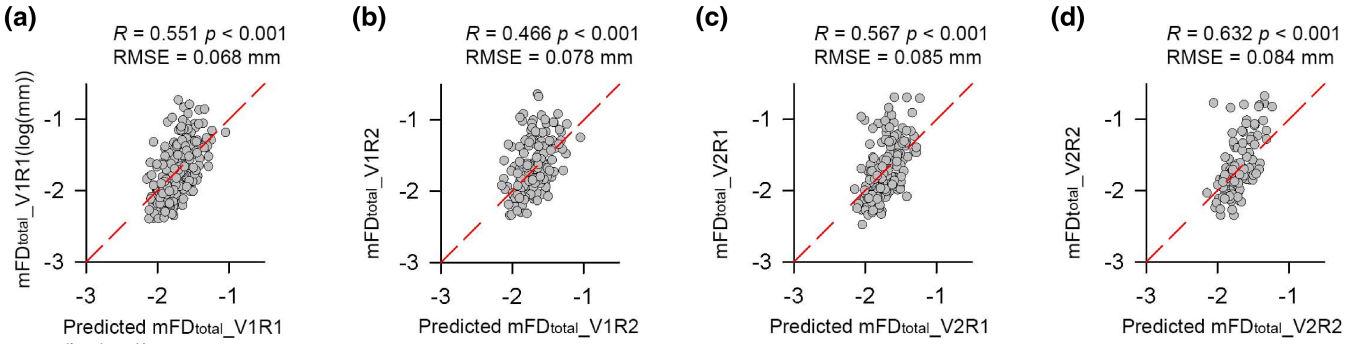

FIGURE 3 The multiple linear regression model derived from V1R1 accurately predicted mFD_{total}s at V1R2, V2R1, and V2R2. (a–d) Scatter plots depicted the performance of the prediction model and showed relationship between predicted mFD_{total} and observed mFD_{total} at V1R1, V1R2, V2R1, and V2R2, respectively.

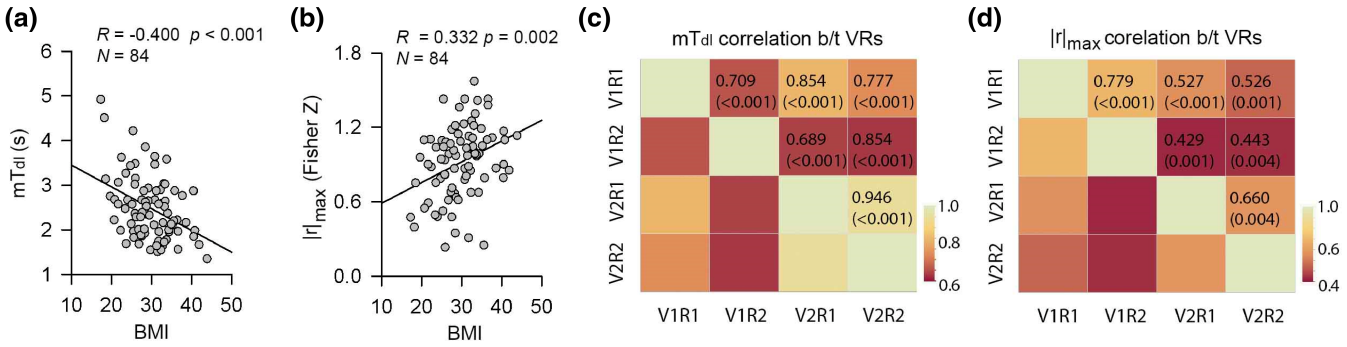

FIGURE 4 BMI was associated with features of the respiration signal, which were stable across scans. (a) Negative association between BMI and mT_{dI} across subjects ($R = -0.400$, $p < 0.001$). (b) Association between BMI and $|r|_{max}$. (c) Association in (a) was consistent across VRs. (d) The association in (b) was consistent across VRs.

duration), and gender accounted for 30.3% of variance of motion at V1R1. BMI was the only significant variable in the model and the ratio of logworth ($-\log_{10}(p)$) to its next closest variable, age ($p = 0.065$), was 12.57. We applied the model built using V1R1 data ($R = 0.551$, $p < 0.001$) to V1R2 ($R = 0.466$, $p < 0.001$), V2R1 ($R = 0.567$, $p < 0.001$), and V2R2 ($R = 0.632$, $p < 0.001$) data. Across scans, BMI was the main determinant of motion across four rs-fMRI scans (Figure 3). In addition, the root mean squared error of motion prediction ranged between 0.068 and 0.085 mm (Figure 3), while mean motion was 0.202 mm. Thus, BMI was the primary predictor of motion across scans.

3.3 | Relationship between respiration and BMI

BMI was significantly associated with two features derived from subjects' respiration signal during the rs-fMRI scanning: the mean time between differentiated inhalations (mT_{dI}) ($R = -0.400$, $p < 0.001$; Figure 4a) and the maximum absolute correlation between dRESP and dMC_{dim}, across six dimensions ($|r|_{max}$) ($R = 0.332$, $p = 0.002$; Figure 4b). In addition, these two significant associations were stable across the four rs-fMRI scans (the range of pair-wise correlations between VRs was between 0.689 and 0.946, all $p < 0.001$; Figure 4c for mT_{dI} and 0.429 and 0.779 and all $p < 0.01$; Figure 4d for $|r|_{max}$),

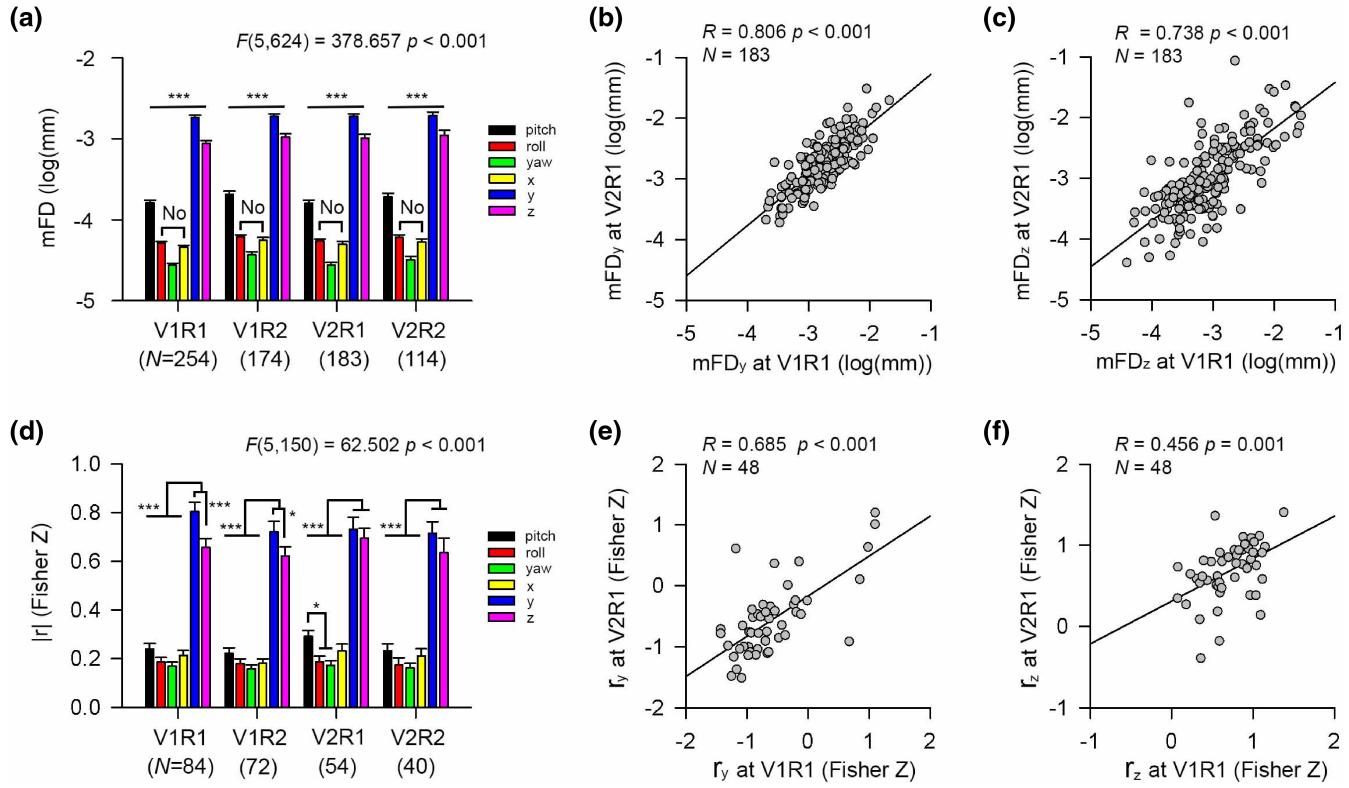

FIGURE 5 Motion in the *y* and *z* dimensions dominated overall motion and the correlations between dRESP and dMC. (a) mFD_y and mFD_z were significantly greater than mFDs of the other four dimensions. (b, c) mFD_y and mFD_z were significantly correlated between V1R1 and V2R1. (d) $|r_y|$ and $|r_z|$ were significantly greater than $|r|$ of other four dimensions. (e, f) Scatter plots showed that r_y and r_z were significantly correlated between at V1R1 and at V2R1, which represented that both magnitude (i.e., $|r|$) and direction of correlation were consistent in *y* and *z* dimensions. Error bar represented s.e.m.; *, **, and *** represented $p < 0.05$, 0.01, and 0.001, respectively.

assuming that the BMI of each subject did not change appreciably between scans. Thus, BMI was significantly associated with the respiration signal and the association was consistent across scans.

3.4 | The relationship between dimension-specific motion and respiration

As shown in Figure 5a, a two-way mixed ANOVA determined that there was a significant main effect of dimension on motion extent ($F(5, 624) = 378.657$, $p < 0.001$) and its post hoc analyses revealed that motion extent in *y* and *z* dimensions (mFD_y and mFD_z) was significantly greater than those in the other four dimensions. The mean ± SD of mFD_y and mFD_z at V1R1 was 0.070 ± 0.028 and 0.056 ± 0.038 mm, respectively, while that of mFD_{pitch}, the next closest one, was 0.026 ± 0.017 mm. Moreover, this domination was consistent across the three other VRs given that mFD_y and mFD_z at V1R1 were significantly correlated with those at V2R2, respectively ($R = 0.806$, $p < 0.001$; Figure 5b for mFD_y and $R = 0.738$, $p < 0.001$; Figure 5c for mFD_y). The domination of motion by the *y* and *z* dimensions was also observed in the correlation between dRESP and dMC_{dim}. As shown in Figure 5d, a two-way mixed ANOVA determined that there was a significant main effect of dimension on motion extent ($F(5, 150) = 62.502$, $p < 0.001$) and its post hoc analyses revealed that the absolute value of correlation between dRESP and dMC_{dim} in *y* and *z* dimension $|r_y|$ and $|r_z|$ was greater than those in the other four dimensions. A consistent domination is also illustrated in Figure 5e for dMC_y and in Figure 5f for dMC_z—the correlation between the correlation (no absolute value here) between dRESP and dMC at V1R1 and at V2R1 was significant ($R = 0.685$, $p < 0.001$ and $R = 0.456$, $p = 0.001$), representing that both extent (i.e., $|r|$) and direction of correlation were consistent in the *y* and *z* dimensions. These results demonstrate that motion in the *y* and *z* dimensions dominated overall motion and the correlations between dRESP and dMC consistently across scans.

3.5 | Relationship between dimension-specific motion, BMI, and respiration

A GEE was fit to assess effects of BMI, $|r_{dim}|$, and their interaction on motion in its corresponding dimension across all four scans. As shown in Table 3 and Figure 6, except the *yaw* dimension, BMI had significant effect on motion and the effect was most pronounced in the *y* and *z* dimensions (Figure 6e,f), consistent with the results in section 3.4. In addition, the GEE revealed that only *pitch* dimension

TABLE 3 Parameter estimates in six dimensions by a generalized estimating equation.

Dimension	Variable	β	SE	t-value	p-value
pitch	BMI	0.016	0.007	6.04	**0.014**
	$\|r\|$	−0.166	0.127	1.71	0.191
	BMI*$\|r\|$	0.041	0.020	4.31	**0.038**
yaw	BMI	0.011	0.006	2.91	0.088
	$\|r\|$	−0.093	0.162	0.33	0.565
	BMI*$\|r\|$	0.004	0.028	0.02	0.885
roll	BMI	0.012	0.004	8.39	**0.004**
	$\|r\|$	0.039	0.128	0.09	0.759
	BMI*$\|r\|$	0.031	0.033	0.91	0.341
x	BMI	0.012	0.006	4.49	**0.043**
	$\|r\|$	0.260	0.129	4.10	0.191
	BMI*$\|r\|$	0.023	0.017	1.97	0.160
y	BMI	0.039	0.005	66.45	**<0.001**
	$\|r\|$	0.060	0.047	1.68	0.190
	BMI*$\|r\|$	−0.007	0.010	0.53	0.470
z	BMI	0.031	0.008	14.63	**<0.001**
	$\|r\|$	0.157	0.119	1.75	0.186
	BMI*$\|r\|$	0.010	0.019	0.29	0.591

Note: Bold p-value represents significant from the statistical analysis (p-value < 0.05).

showed an appreciable interaction between BMI and $|r_{pitch}|$ ($p = 0.038$). Figure 6a clearly illustrates the effect of the interaction: when BMI was on the left side of the red line, as $|r_{pitch}|$ increased, motion decreased; however, the effect of $|r_{pitch}|$ on motion was opposite when BMI was on the right side of the red line. These results show that BMI and absolute correlation interact to affect motion in the *pitch* dimension.

4 | DISCUSSION

Here, we reconfirmed patients with back pain have head motion that is stable across scans within an individual but varies significantly across individuals. We revealed that (1) BMI was the main determinant in predicting motion and was significantly associated with respiration signal, (2) *y* and *z* dimensions dominated overall motion and the correlation between dRESP and dMC, and (3) BMI and $|r|$ interact to affect motion in the *pitch* dimension.

Even though the pain intensity of the second visit was lower compared to the first one ($F(1,434) = 42.891$, $p < 0.001$), for both visits, we replicated our prior finding that pain intensity is significantly correlated to head motion for patients with back pain (Huang et al., 2019; Yang et al., 2021). However, the variance in head motion explained by pain is low compared to BMI insofar as BMI is the only significant variable to predict motion across scans in the multiple linear regression analysis. The discomfort caused by back pain may consistently contribute to motion, so the correlations between scans are greater (0.76–0.86) than healthy controls (0.53–0.66) in previous studies (Hodgson et al., 2017). Thus, although it is necessary to take preventive strategies, like educating participants to reduce anxiety before scanning (Zaitsev et al., 2015) or other constraint methods to reduce motion in each scan—which we discuss in more detail later in the discussion—BMI should be included as a pivotal factor in recruitment, fMRI data quality control, and statistical analysis for pain fMRI study.

This study quantitatively linked BMI with two features derived from the respiration signal that was synchronized with image scanning and suspected to be related to head motion during image acquisition. The observation that individuals' BMI is significantly associated with the differentiated inhalation signal (and also inhalation signal in our data) instead of that of the exhalation signal is consistent with the finding that there is decreased in inhalation time but unvaried exhalation time for the obese individuals (Sampson & Grassino, 1983). Another significant association with BMI is $|r|_{max}$, representing the dynamic coupling strength between motion and respiration during image acquisition. BMI augments motion's coupling with respiration and its effect on motion may be so great that it dwarfs other factors, for example, impulsivity (Couvy-Duchesne et al., 2016; Kong et al., 2014), pain intensity (Huang et al., 2019; Yang et al., 2021), and age (Mowinckel et al., 2012). With these two associations, an increase of inhalation time and a decrease of coupling between motion and respiration can be predicted following weight loss (Beyer et al., 2020). Furthermore, the significant association between the BMI and the two features, along with evidence of shared genetic influences between head motion and BMI (Hodgson et al., 2017; Zhou et al., 2016), may indicate that respiration is physiologically linked with head motion and BMI. However, besides the respiration, we cannot exclude the effect of other factors related to BMI on motion, such as participants' feeling cramped in the scanner, especially for the subjects with greater BMI—assessing this feeling is an interesting avenue for future work. Yet, we surmise that the movement caused by the feeling might be less than that caused by chronic back pain, the latter of which was significantly correlated with mFD (Figure 2e).

MCFLIRT provides us with not only estimates of mean motion over the entire acquisition period but also that of extent and direction of motion in 6 different motion dimensions, arming us to improve existing pre-acquisition strategies and introducing new avenues to mitigate motion effects. The significant domination of the *y* (anterior–posterior) and *z* (superior–inferior) dimensions in motion magnitude, its coupling strength between motion and respiration, and its consistence across scans can partly be explained by the restraint by two foam pads positioned on either side of the head, which restrains subjects from moving left–right and rotating on both anterior–posterior and superior–inferior axes. This finding can help explain how active motion reduction strategies work and lend insight for improvements, such as taping the forehead of subjects for tactile feedback (Krause et al., 2019). Having direct feedback not only reminds subject to keep their head still but also restrains subjects' head from moving in the *y* and *z* dimensions, along with suppressing rotation along the *pitch* dimension, greatly reducing motion. If the

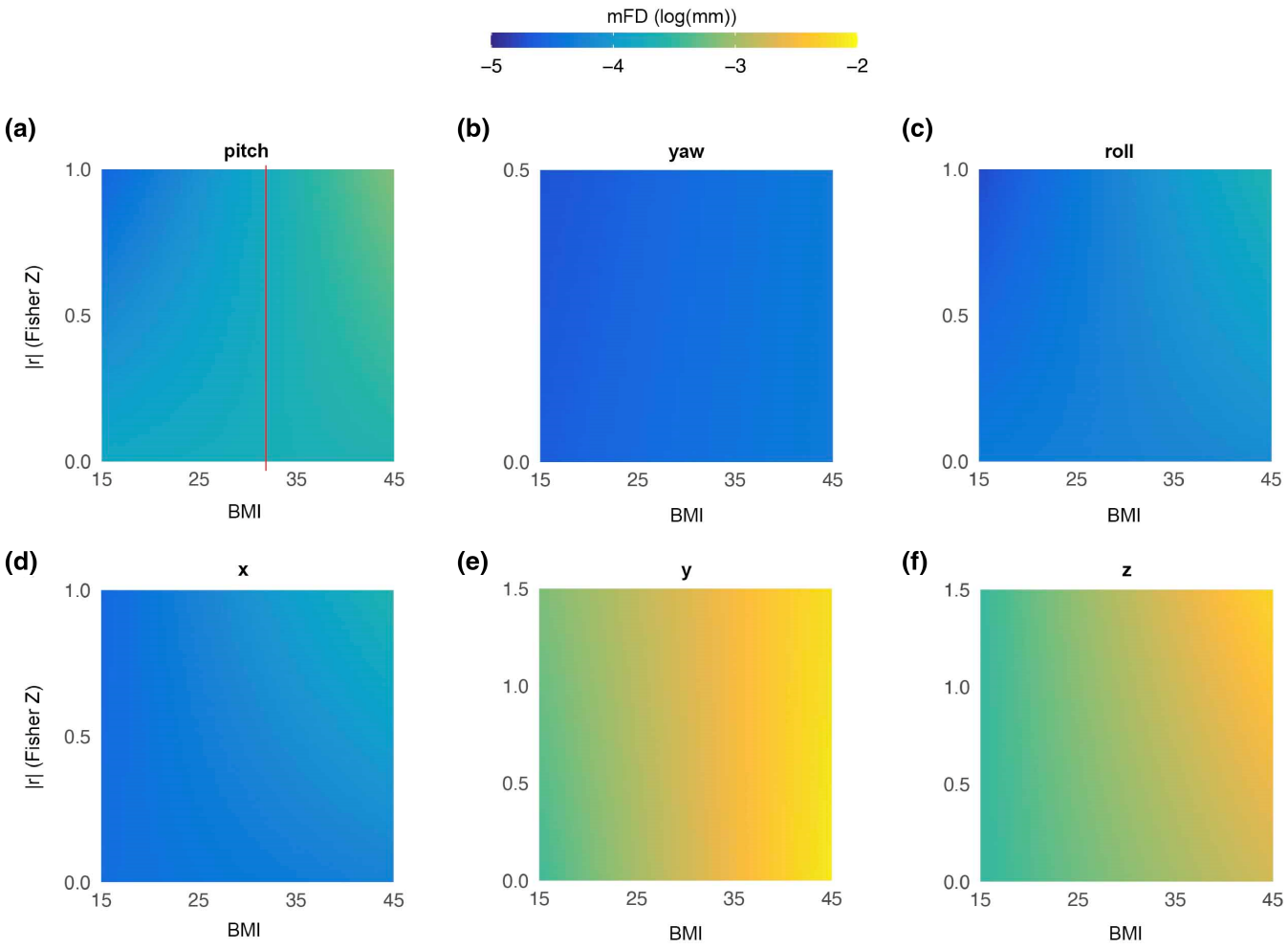

FIGURE 6 Generalized estimating equations predicted motions (mFD) within the space spanned by BMI and |*r*| in its corresponding dimension.

medical tape is replaced by a stronger physical restraint (e.g., elastic band or nylon straps), its effect may be more striking because it will significantly disrupt the coupling between motion and respiration in the *y*, *z*, and *pitch* dimensions. Another pre-acquisition strategy involves a 3D printer to generate customized molds to physically restrain participants' heads from moving in any dimension (Power et al., 2019). Considering the cost and time associated with 3D printing, unless for some very special populations, like patients with a rare disease or tremors/ticks, a more practical strategy is to redesign foam pads and find optimal numbers and positions to support the head by evaluating the interaction between BMI and |*r*| and its effects on motion in each dimension.

5 | LIMITATIONS

First, BMI was assumed to be unvaried between two visits for the four scans, but 59 of 254 participants (23.23%) had greater than 6-month interval time between the two visits, so we cannot exclude the possibility of violation of the assumption. Second, due to lack of the BMI in the second visit, we are unable to explore the causal link(s) among BMI, respiration, and head motion. Third, although we observed an interaction between |*r*| and BMI affecting motion extent only in the *pitch* dimension, we had not proposed a scientific and reasonable explanation, which needs to be further investigated. In the future, we will further illuminate the relationships between BMI, respiration, and motion in a larger data set (e.g., HCP; Van Essen, Ugurbil et al., 2012; Van Essen, Smith et al., 2013), where we hope to identify a better denoising strategy for mitigating the effect of motion.

6 | CONCLUSIONS

In clinical fMRI research, head motion is nearly always a confound, and this confound is amplified in populations with high BMI. We demonstrate that, in a patient population (chronic pain), these motion effects are repeatable and substantial, dominating the effects of age and pain intensity. Moreover, this BMI effect interacted with respiration in a dimension-specific manner. More work is necessary to

explore the generalizability of these findings, especially in other patient populations.

ACKNOWLEDGMENTS

We thank NIH (grant 1P50DA044121-01A1) for funding data analysis. This material is based upon work supported by the National Science Foundation Graduate Research Fellowship under Grant No. DGE-1324585.

CONFLICT OF INTEREST STATEMENT

The authors declare no conflicts of interest.

DATA AVAILABILITY STATEMENT

An excerpt of the data and scripts related were uploaded to OpenPain.org and https://github.com/lejianhuang/Motion-Respiration-BMI/. The imaging dataset in this article is part of a multiphase project which is still under investigation. It will eventually be made available in OpenPain.org once the multiphase project is complete.

ORCID

Apkar Vania Apkarian https://orcid.org/0000-0002-9788-7458
Lejian Huang https://orcid.org/0000-0003-1753-2372

REFERENCES

Beyer, F., Prehn, K., Wusten, K. A., Villringer, A., Ordemann, J., Floel, A., & Witte, A. V. (2020). Weight loss reduces head motion: Revisiting a major confound in neuroimaging. *Human Brain Mapping*, *41*(9), 2490–2494.

Ciric, R., Rosen, A. F. G., Erus, G., Cieslak, M., Adebimpe, A., Cook, P. A., Bassett, D. S., Davatzikos, C., Wolf, D. H., & Satterthwaite, T. D. (2018). Mitigating head motion artifact in functional connectivity MRI. *Nature Protocols*, *13*(12), 2801–2826.

Couvy-Duchesne, B., Blokland, G. A., Hickie, I. B., Thompson, P. M., Martin, N. G., de Zubicaray, G. I., McMahon, K. L., & Wright, M. J. (2014). Heritability of head motion during resting state functional MRI in 462 healthy twins. *NeuroImage*, *102*(Pt 2), 424–434.

Couvy-Duchesne, B., Ebejer, J. L., Gillespie, N. A., Duffy, D. L., Hickie, I. B., Thompson, P. M., Martin, N. G., de Zubicaray, G. I., McMahon, K. L., Medland, S. E., & Wright, M. J. (2016). Head motion and inattention/hyperactivity share common genetic influences: Implications for fMRI studies of ADHD. *PLoS One*, *11*(1), e0146271.

Ekhtiari, H., Kuplicki, R., Yeh, H. W., & Paulus, M. P. (2019). Physical characteristics not psychological state or trait characteristics predict motion during resting state fMRI. *Scientific Reports*, *9*, 419.

Farrar, J. T., Young, J. P., Jr., LaMoreaux, L., Werth, J. L., & Poole, R. M. (2001). Clinical importance of changes in chronic pain intensity measured on an 11-point numerical pain rating scale. *Pain*, *94*(2), 149–158.

Halekoh, U., Hojsgaard, S., & Yan, J. (2006). The R package geepack for generalized estimating equations. *Journal of Statistical Software*, *15*(2), 1–11.

Hodgson, K., Poldrack, R. A., Curran, J. E., Knowles, E. E., Mathias, S., Goring, H. H. H., Yao, N., Olvera, R. L., Fox, P. T., Almasy, L., Duggirala, R., Barch, D. M., Blangero, J., & Glahn, D. C. (2017). Shared genetic factors influence head motion during MRI and body mass index. *Cerebral Cortex*, *27*(12), 5539–5546.

Hoinkiss, D. C., Erhard, P., Breutigam, N. J., von Samson-Himmelstjerna, F., Gunther, M., & Porter, D. A. (2019). Prospective motion correction in functional MRI using simultaneous multislice imaging and multislice-to-volume image registration. *NeuroImage*, *200*, 159–173.

Huang, S., Wakaizumi, K., Wu, B., Shen, B., Wu, B., Fan, L., Baliki, M. N., Zhan, G., Apkarian, A. V., & Huang, L. (2019). Whole-brain functional network disruption in chronic pain with disk herniation. *Pain*, *160*(12), 2829–2840.

Hucker, P., Dacko, M., & Zaitsev, M. (2021). Combining prospective and retrospective motion correction based on a model for fast continuous motion. *Magnetic Resonance in Medicine*, *86*, 1284–1298.

Igata, N., Kakeda, S., Watanabe, K., Nozaki, A., Rettmann, D., Narimatsu, H., Ide, S., Abe, O., & Korogi, Y. (2017). Utility of real-time prospective motion correction (PROMO) for segmentation of cerebral cortex on 3D T1-weighted imaging: Voxel-based morphometry analysis for uncooperative patients. *European Radiology*, *27*(8), 3554–3562.

Jenkinson, M., Bannister, P., Brady, M., & Smith, S. (2002). Improved optimization for the robust and accurate linear registration and motion correction of brain images. *NeuroImage*, *17*(2), 825–841.

Kong, X. Z., Zhen, Z., Li, X., Lu, H. H., Wang, R., Liu, L., He, Y., Zang, Y., & Liu, J. (2014). Individual differences in impulsivity predict head motion during magnetic resonance imaging. *PLoS One*, *9*(8), e104989.

Krause, F., Benjamins, C., Eck, J., Luhrs, M., van Hoof, R., & Goebel, R. (2019). Active head motion reduction in magnetic resonance imaging using tactile feedback. *Human Brain Mapping*, *40*(14), 4026–4037.

Lee, C. C., Jack, C. R., Jr., Grimm, R. C., Rossman, P. J., Felmlee, J. P., Ehman, R. L., & Riederer, S. J. (1996). Real-time adaptive motion correction in functional MRI. *Magnetic Resonance in Medicine*, *36*(3), 436–444.

Liang, K. Y., & Zeger, S. L. (1986). Longitudinal data-analysis using generalized linear-models. *Biometrika*, *73*(1), 13–22.

Mafort, T. T., Rufino, R., Costa, C. H., & Lopes, A. J. (2016). Obesity: Systemic and pulmonary complications, biochemical abnormalities, and impairment of lung function. *Multidisciplinary Respiratory Medicine*, *11*, 28.

Mowinckel, A. M., Espeseth, T., & Westlye, L. T. (2012). Network-specific effects of age and in-scanner subject motion: A resting-state fMRI study of 238 healthy adults. *NeuroImage*, *63*(3), 1364–1373.

Paik, M. C. (1988). Repeated measurement analysis for nonnormal data in small samples. *Communications in Statistics-Simulation and Computation*, *17*(4), 1155–1171.

Pinto, C. B., Bielefeld, J., Barroso, J., Yip, B., Huang, L. J., Schnitzer, T., & Apkarian, A. V. (2023). Chronic pain domains and their relationship to personality, abilities, and brain networks. *Pain*, *164*(1), 59–71.

Power, J. D., Mitra, A., Laumann, T. O., Snyder, A. Z., Schlaggar, B. L., & Petersen, S. E. (2014). Methods to detect, characterize, and remove motion artifact in resting state fMRI. *NeuroImage*, *84*, 320–341.

Power, J. D., Silver, B. M., Silverman, M. R., Ajodan, E. L., Bos, D. J., & Jones, R. M. (2019). Customized head molds reduce motion during resting state fMRI scans. *NeuroImage*, *189*, 141–149.

Pruim, R. H. R., Mennes, M., van Rooij, D., Llera, A., Buitelaar, J. K., & Beckmann, C. F. (2015). ICA-AROMA: A robust ICA-based strategy for removing motion artifacts from fMRI data. *NeuroImage*, *112*, 267–277.

Reckziegel, D., Tetreault, P., Ghantous, M., Wakaizumi, K., Petre, B., Huang, L., Jabakhanji, R., Abdullah, T., Vachon-Presseau, E., Berger, S., Baria, A., Griffith, J. W., Baliki, M. N., Schnitzer, T. J., & Apkarian, A. V. (2021). Sex-specific pharmacotherapy for Back pain: A proof-of-concept randomized trial. *Pain and Therapy*, *10*(2), 1375–1400.

Salimi-Khorshidi, G., Douaud, G., Beckmann, C. F., Glasser, M. F., Griffanti, L., & Smith, S. M. (2014). Automatic denoising of functional MRI data: Combining independent component analysis and hierarchical fusion of classifiers. *NeuroImage*, *90*, 449–468.

Sampson, M. G., & Grassino, A. E. (1983). Load compensation in obese patients during quiet tidal breathing. *Journal of Applied Physiology*, *55*(4), 1269–1276.

Tetreault, P., Mansour, A., Vachon-Presseau, E., Schnitzer, T. J., Apkarian, A. V., & Baliki, M. N. (2016). Brain connectivity predicts placebo response across chronic pain clinical trials. *PLoS Biology*, *14*(10), e1002570.

Todd, N., Josephs, O., Callaghan, M. F., Lutti, A., & Weiskopf, N. (2015). Prospective motion correction of 3D echo-planar imaging data for functional MRI using optical tracking. *NeuroImage*, *113*, 1–12.

Van Essen, D. C., Smith, S. M., Barch, D. M., Behrens, T. E., Yacoub, E., Ugurbil, K., & WU-Minn HCP Consortium. (2013). The WU-Minn human connectome project: An overview. *NeuroImage*, *80*, 62–79.

Van Essen, D. C., Ugurbil, K., Auerbach, E., Barch, D., Behrens, T. E., Bucholz, R., Chang, A., Chen, L., Corbetta, M., Curtiss, S. W., Penna, S. D., Feinberg, D., Glasser, M. F., Harel, N., Heath, A. C., Larson-Prior, L., Marcus, D., Michalareas, G., Moeller, S., … WU-Minn HCP Consortium. (2012). The human connectome project: A data acquisition perspective. *NeuroImage*, *62*(4), 2222–2231.

Yang, L., Wu, B., Fan, L., Huang, S., Vigotsky, A. D., Baliki, M. N., Yan, Z., Apkarian, A. V., & Huang, L. (2021). Dissimilarity of functional connectivity uncovers the influence of participant's motion in functional magnetic resonance imaging studies. *Human Brain Mapping*, *42*(3), 713–723.

Zaitsev, M., Maclaren, J., & Herbst, M. (2015). Motion artifacts in MRI: A complex problem with many partial solutions. *Journal of Magnetic Resonance Imaging*, *42*(4), 887–901.

Zeng, L. L., Wang, D., Fox, M. D., Sabuncu, M., Hu, D., Ge, M., Buckner, R. L., & Liu, H. (2014). Neurobiological basis of head motion in brain imaging. *Proceedings of the National Academy of Sciences of the United States of America*, *111*(16), 6058–6062.

Zhou, Y., Chen, J., Luo, Y. L. L., Zheng, D., Rao, L.-L., Li, X., Zhang, J., Li, S., Friston, K., & Zuo, X.-N. (2016). Genetic overlap between in-scanner head motion and the default network connectivity. bioRxiv preprint: https://doi.org/10.1101/087023

How to cite this article: Huang, S., Vigotsky, A. D., Apkarian, A. V., & Huang, L. (2024). Body mass index associated with respiration predicts motion in resting-state functional magnetic resonance imaging scans. *Human Brain Mapping*, *45*(13), e70015. https://doi.org/10.1002/hbm.70015